Journal of Sound and Vibration 372 (2016) 31–49

Contents lists available at ScienceDirect

Journal of Sound and Vibration

journal homepage: www.elsevier.com/locate/jsvi

Spectral matrix completion by Cyclic Projection and application to sound source reconstruction from non-synchronous measurements

Liang Yu *, Jerome Antoni, Quentin Leclere

Laboratory Vibrations and Acoustics, INSA-Lyon, Batiment St. Exupery 25 bis av. Jean Capelle, 69621 Villeurbanne cedex, France

ARTICLE INFO

Article history:
Received 28 April 2015
Received in revised form
16 February 2016
Accepted 16 February 2016
Handling Editor: K. Shin
Available online 4 March 2016

Keywords:
Inverse acoustic problem
Sequential measurements
Structured low rank model
Cyclic projection

ABSTRACT

A fundamental limitation of the inverse acoustic problem is determined by the size of the array and the microphone density. A solution to achieve large array and/or high microphone density is to scan the object of interest by moving sequentially a small prototype array, which is referred to as sequential measurements. In comparison to a large array and/or high microphone density array that can acquire simultaneously all the information of the spectral matrix, in particular all cross-spectra, sequential measurements can only acquire a block diagonal spectral matrix, while the cross-spectra between the sequential measurements remain unknown due to the missing phase relationships between consecutive positions. Nevertheless, these unknown cross-spectra are necessary for sound source reconstruction. The objective of this paper is to propose an algorithm to recover the missing elements of the spectral matrix in the case where the acoustical field is highly coherent. This issue is shown to boil down to a matrix completion problem subject to given constraint of hermitian symmetry, measurements fitting, reduced rank and spatial continuity of the sound field. A Cyclic Projection (CP) algorithm is proposed in this work to find an optimal solution at the intersection between three predefined sets. The proposed method is analyzed through numerical simulations of diverse setups and is also validated experimentally.

1. Introduction

Sound source reconstruction aims at characterizing acoustical sources that radiate at certain distance from partial measurements of the pressure field. In general, measurements are taken with a microphone array whose dimensions and density are circumscribed due to obvious cost and technical reasons; this brings about strong limitations on the reconstruction capability in terms of spatial resolution and magnitude quantification. In Near-Field Acoustic Holography (NAH) [1], it is assumed that the measurement aperture is infinite in theory for the purpose of guaranteeing the reconstruction quality. However in practice, a limited measurement aperture is only available to cover a part of the radiating region, which results in truncation effects, wrap-around errors and other errors due to the discontinuity of the aperture edge [2,3]. In order to breakthrough this crucial limitation, the patch holography method has been proposed [4–6]; it consists in extrapolating the acoustic field outside the aperture from the hologram data that are measured within the aperture [7]. In patch holography, the spatial spectra of the measured pressures (or particle velocity) are assumed to be band-limited in the

* Corresponding author.

http://dx.doi.org/10.1016/j.jsv.2016.02.031
0022-460X/

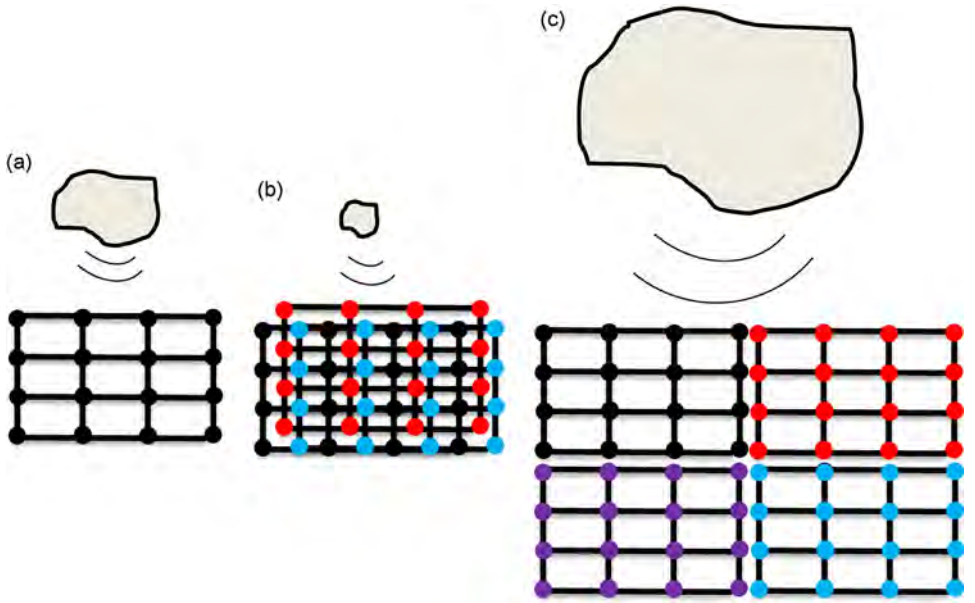

Fig. 1. (a) Measurement with a prototype array. (b) Sequential measurements for making the array denser, (c) Sequential measurements for making the array larger.

wavenumber space (K-space) [8], which implies a certain degree of spatial correlation between the measurement positions. Put differently, the closer the spatial positions, the more the acoustical field is correlated which allows a smooth-and-replace alternating projection [6,9] to reconstruct the hologram data that are not directly measured. In Ref. [10], the assumption of a sparse spectrum is investigated instead of the band-limited assumption, which provides another perspective to investigate the extrapolation of the acoustical field. This is further investigated to achieve super-resolution reconstruction in Refs. [11,12].

Another solution to achieve a large array and/or high microphone density is to scan the object of interest by moving sequentially a small prototype array, which is referred to as sequential measurements. A small prototype array is moved along different locations in front of or around the radiating object to augment the microphone density or the measurement aperture size. For instance, Fig. 1(a) shows a prototype array that is optimized to a given configuration as compared with the source dimensions, Fig. 1(b) shows how to use sequential measurements to make the array denser, and Fig. 1(c) how to make the array larger. Contrary to simultaneous measurements, sequential measurements are faced with the difficulty that phase relationships are lost between consecutive measurements, yet such information is vital to signal reconstruction in general [13,14]. One strategy to tackle such a problem is to use a set of fixed reference microphones located in the acoustical field which are fully correlated with the sources so as to indirectly measure phase relationships between consecutive positions of the array; then phases that are lost can be reconstructed by spectral analysis based methods (Conditioned Spectral Analysis and Principal Component Analysis) [15,16]. A related method that is based on a linear prediction technique is proposed based on the same fixed references strategy in Ref. [17].

However, the effectiveness of these approaches is strongly dependent on the availability of high-quality references (high signal-to-noise ratios and high coherence with the source field) in sufficient number to capture the stochastic dimension of the source field (i.e. the number of uncorrelated sources it is composed of); in particular the number of references should be greater than or equal to the number of uncorrelated sources. Unfortunately, the provision of references incurs an extra cost and precludes some microphones to be used when the user has to face a limited number of tracks in the acquisition system. Broadband acoustic holography from intensity measurements (BAHIM) [18] breaks through the restriction of using references by reconstructing the phase from the quadratic pressure and tangential components of sound intensity. BAHIM has been extended to the scenario with disturbing sources on the opposite of the hologram plane in Ref. [19]. An alternative version of BAHIM with improved accuracy in detecting and localizing the sources is recently presented in [20].

Sequential measurements from pressure measurements without reference have been addressed in Ref. [21]. In comparison with a large array and/or high microphone density array that can acquire simultaneously all the spectral matrix, sequential measurements can only acquire a block diagonal spectral matrix that comprises auto-spectra, while some of the cross-spectra remain unknown due to the missing phase relationships between consecutive array positions. In Ref. [21], the incomplete measurements (data missing spectral matrix) are explicitly taken into account in solving an inverse problem to reconstruct the source distribution. The objective of this paper is to propose a solution fundamentally different from the state-of-the-art, which aims to complete a data missing spectral matrix prior to using it for sound source reconstruction. The approach is therefore referred to as non-intrusive, a flexibility which should offer larger perspectives of application. The spectral matrix completion is recognized as an ill-posed inverse problem [22] since only the diagonal blocks of the spectral

matrix are acquired, which contain much less elements than the unknowns of the full matrix that are searched. Thus, some extra conditions (regularization) need to be adjoined to solve the problem. In this paper, the high correlation of the acoustical field is considered as the core physical assumption, and it is characterized by means of two specific properties:

1. *Low rank spectral matrix*: The rank of the spectral matrix is consistent with the number of "virtual source", i.e. the number of equivalent uncorrelated sources the acoustical field comprises.
2. *Continuity of the acoustic field*: It implies that two columns of the spectral matrix tend to become identical as the corresponding microphone positions become arbitrarily close to each other.

The paper is organized as follows. In Section 2, the forward problem model is first defined. In Section 3, the problem is formally formulated as a structured low rank model and its ingredients are explained in separate subsections. A Cyclic Projection algorithm is proposed to solve the structured low rank model in Section 4. Sections 5 and 6 deal with parameter analysis results and experimental validation. The conclusion is in Section 7.

2. Stochastic modeling of the forward problem

2.1. Stochastic modeling of sequential measurements

Let $s(\mathbf{r},\omega;\zeta), \mathbf{r}\in\Gamma$ be the normal velocity or acoustic pressure on the source surface Γ enclosing the radiating object D, at a given frequency ω. The fundamental premise is that the acoustic source distribution is considered as a stationary stochastic field, thus the acoustic sources produce outcomes whose realizations depend on the events ζ in sample space Ω. From a practical point of view (assumption of ergodicity), an outcome of the source distribution will simply correspond to a snapshot of the measured signal (i.e. the Fourier transform of a short-time segment possibly tapered with a smooth data window) at a given position of the array.

The acoustic field that is produced by the radiating body D is measured at some discrete locations $r_{m,i}$, where $r_{m,i}$ denotes the position of the m-th microphone in the array, $m=1,\ldots,M$ at the i-th position of the array, $i=1,\ldots,P$ (an array of M microphones with P measurements), and $p(r_{m,i},\omega;\zeta)$ is the acoustic pressure measured at this point (see Fig. 2). Note that for a given array position i, M measurements are taken simultaneously. Similarly, for a given microphone m, the P measurements that result from moving the array at different positions are sequential; this implies that phase relationships between measurements at points $p(r_{m,i},\omega;\zeta)$ and $p(r_{n,j},\omega;\zeta')$, $\forall(n,m), i\neq j$, are necessarily lost.

Having defined the measured pressures and the source field, the direct problem typically relates them through an integral equation of the form

$$p(r_{m,i},\omega;\zeta)=\int_{\Gamma} G(r_{m,i},\omega|\mathbf{r})s(\mathbf{r},\omega;\zeta)\,\mathrm{d}\Gamma(\mathbf{r})+n(r_{m,i},\omega;\zeta), \tag{1}$$

where $G(r_{m,i},\omega|\mathbf{r})$ denotes the Green function (provided in analytical or numerical form) between $\mathbf{r}$ and $r_{m,i}$, and where $n(r_{m,i},\omega;\zeta)$ stands for additive measurement noise statistically independent of $s(\mathbf{r},\omega;\zeta)$. In order to discretize the problem, let us project it onto a basis of spatial functions $\{\phi_k(\mathbf{r},\omega)\}_{k=1}^{K}$ whose choice may be either arbitrary or optimal [23] given the

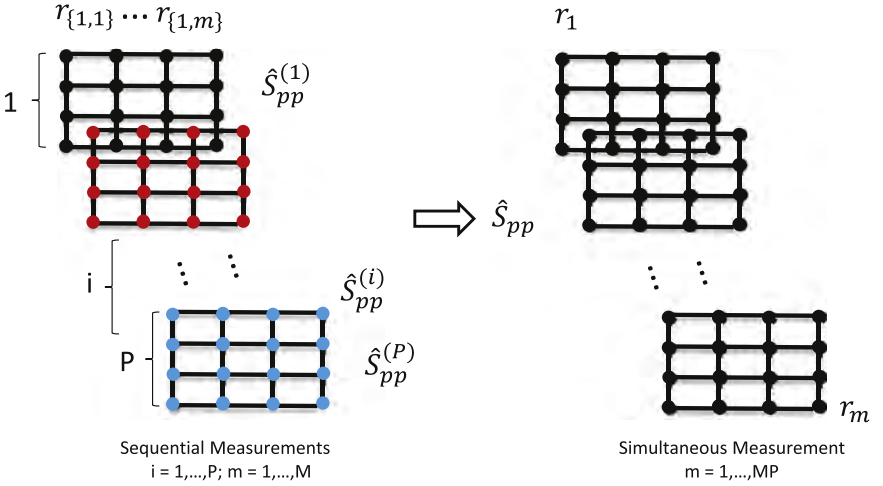

Fig. 2. Sequential measurements versus simultaneous measurement (measurement mode).

object and array geometries:

$$s(\mathbf{r},\omega;\zeta)=\sum_{k=1}^{K}c_k(\zeta)\phi_k(\mathbf{r},\omega). \tag{2}$$

For a given frequency ω, coefficients $c_k(\zeta)$ assigned to the basis functions $\phi_k(\mathbf{r},\omega)$ are to be interpreted as K random variables that produce the stochastic field $s(\mathbf{r},\omega;\zeta)$. Eq. (1) then becomes

$$p(r_{m,i},\omega;\zeta)=\sum_{k=1}^{K}H_{m,i,k}c_k(\zeta)+n(r_{m,i},\omega;\zeta), \tag{3}$$

where

$$H_{m,i,k}=\int_{\Gamma}G(r_{m,i},\omega|\mathbf{r})\phi_k(\mathbf{r},\omega)\,\mathrm{d}\Gamma(\mathbf{r})$$

is interpreted as a transfer function. Eq. (3) can be recast into a more compact form. Let N_i be the number of snapshots available at position i , $\mathbf{p}_{ij}\in\mathbb{C}^M$ the column vector containing the M pressures $\{p(r_{m,i},\omega;\zeta)\}_{m=1}^{M}$ measured at the j-th snapshot and i-th position of the array, $\mathbf{c}_{ij}\in\mathbb{C}^K$ the column vector containing the K coefficients $\{c_k(\zeta_{ij})\}_{k=1}^{K}$, $\mathbf{n}_{ij}\in\mathbb{C}^M$ the column vector of additive noises $\{n(r_{m,i},\omega;\zeta_{ij})\}_{m=1}^{M}$ and $\mathbf{H}_i\in\mathbb{C}^{M\times K}$ the matrix with elements $[H_i]_{mk}=H_{m,i,k}$. The matrix version of Eq. (3) then reads

$$\mathbf{p}_{ij}=\mathbf{H}_i\mathbf{c}_{ij}+\mathbf{n}_{ij},\quad m=1,\ldots,M,\ \ i=1,\ldots,P, \tag{4}$$

where $\mathbf{n}_{ij}$ has covariance matrix $\beta_i^2\mathbf{\Omega}_i$ with assumed spatial coherence $\mathbf{\Omega}_i$ normalized such that its trace $\mathrm{tr}\{\mathbf{\Omega}_i\}=M$ and where the noise power β_i^2 is an unknown hyper-parameter.

Let us define the expected value of any function $f^{(i)}$, evaluated at the i-th position of the array, as

$$\mathbb{E}\{f^{(i)}\}=\lim_{N\to\infty}\frac{1}{N}\sum_{j=1}^{N}f^{(i)}\left(\zeta_{ij}\right). \tag{5}$$

Next, let $\mathbf{S}_{pp}^{(i)}\doteq\mathbb{E}\{\mathbf{p}_{ij}\mathbf{p}_{ij}^{*}\}$ (with $*$ being the transpose-conjugate operator) define the spectral matrix of the measurements at position i, whose diagonal (resp. off-diagonal) elements contain the auto (resp. cross) spectra of the measured pressures. Similarly, let $\mathbf{S}_{cc}\doteq\mathbb{E}\{\mathbf{c}_{ij}\mathbf{c}_{ij}^{*}\}$ be the covariance matrix of the unknown coefficients, which does not depend on index i by definition of the source field stationarity. Let us also introduce

$$\hat{\mathbf{S}}_{pp}^{(i)}=\frac{1}{N_i}\sum_{j=1}^{N_i}\mathbf{p}_{ij}\mathbf{p}_{ij}^{*}, \tag{6}$$

an estimate of the theoretical spectral matrix $\mathbf{S}_{pp}^{(i)}$ obtained by averaging the outer-product of measured pressure vectors over a finite number of snapshots. Therefore, it results from Eq. (6) that

$$\hat{\mathbf{S}}_{pp}^{(i)}\simeq\mathbf{H}_i\mathbf{S}_{cc}\mathbf{H}_i^{*}+\beta_i^2\mathbf{\Omega}_i,\quad i=1,\ldots,P, \tag{7}$$

with exact equality when the number of snapshots tends to infinity, $N_i\to\infty$. These covariance equations physically reflect transfer of energy from the source field to the microphones.

2.2. Stochastic modeling of simultaneous measurement

In the simultaneous measurement, Eq. (4) can be directly written as follows (without subscript i since measurements are captured simultaneously) in a vector form:

$$\mathbf{p}_j=\mathbf{H}\mathbf{c}_j+\mathbf{n}_j. \tag{8}$$

The theoretic spectral matrix $\mathbf{S}_{pp}$ of simultaneous measurement is then $\mathbf{S}_{pp}\doteq\mathbb{E}\{\mathbf{p}_j\mathbf{p}_j^{*}\}=\mathbf{H}\mathbb{E}\{\mathbf{c}_j\mathbf{c}_j^{*}\}\mathbf{H}^{*}+\mathbb{E}\{\mathbf{n}_j\mathbf{n}_j^{*}\}$, where $\mathbb{E}\{\mathbf{n}_j\mathbf{n}_j^{*}\}=\sigma_n^2\mathbf{\Omega}$ and the definition of $\mathbf{S}_{cc}\doteq\mathbb{E}\{\mathbf{c}_{ij}\mathbf{c}_{ij}^{*}\}=\mathbb{E}\{\mathbf{c}_j\mathbf{c}_j^{*}\}$ (independent of i) remains the same as in the sequential measurements owing to the stationarity assumption of source field. Similar to sequential measurements, $\hat{\mathbf{S}}_{pp}=\frac{1}{N}\sum_{j=1}^{N}\mathbf{p}_j\mathbf{p}_j^{*}$; then Eq. (8) can be written as:

$$\hat{\mathbf{S}}_{pp}\simeq\mathbf{S}_{pp}^{L}+\sigma_n^2\mathbf{\Omega}=\mathbf{H}\mathbf{S}_{cc}\mathbf{H}^{*}+\sigma_n^2\mathbf{\Omega}, \tag{9}$$

where σ_n^2 is the noise power in simultaneous measurements, $\mathrm{tr}(\mathbf{\Omega})=\mathrm{MP}$, and $\mathbf{\Omega}$ is a diagonal matrix by assuming that the noise in different channels is uncorrelated. The equality is exact when the number of snapshots N tends to infinity. It is assumed that $\mathbf{S}_{pp}^{L}=\mathbf{H}\mathbf{S}_{cc}\mathbf{H}^{*}$ is a low rank matrix, where $\mathbf{H}$ is full row rank and $\mathrm{rank}(\mathbf{H}\mathbf{S}_{cc}\mathbf{H}^{*})=\mathrm{rank}(\mathbf{S}_{cc})$.

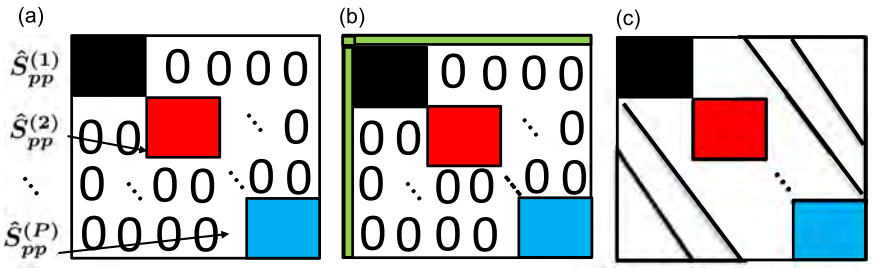

Fig. 3. Structure of the spectral matrix in the case of (a) sequential measurements without reference (data missing matrix), (b) sequential measurements with references (data missing matrix), and (c) simultaneous measurement (full matrix).

2.3. Problem statement

An essential question to be addressed now is the difference between sequential measurements and simultaneous measurements from the spectral matrix perspective. With sequential measurement, an incomplete spectral matrix $\hat{\mathbf{S}}_{pp}^{m}$ is constructed by rearranging all spectral sub-matrices $\hat{\mathbf{S}}_{pp}^{(i)}$, $i=1,\ldots,P$, in Eq. (7) (each with size $M\times M$) methodically in block diagonal positions and the remaining positions are padded by zero elements (see Fig. 3(a), note that zero padding is a just a way to visualize the unknown part of the measured matrix). Contrary to sequential measurements, $\hat{\mathbf{S}}_{pp}$ in Eq. (9) is a complete matrix as shown in Fig. 3(c). With the purpose of using sequential measurements for sound source, the problem is to complete a full spectral matrix from the data missing spectral matrix $\hat{\mathbf{S}}_{pp}^{m}$. In fact, the spectral matrix in sequential measurements with references is also a data missing matrix but with known cross-spectra between the references and each sequential measurement, as illustrated in Fig. 3(b). Thus, when the problem is formulated as a matrix completion, it is general enough to cover the two cases with and without references.

3. Structured low-rank completion problem

In order to solve the matrix completion problem, the following optimization is proposed:

$$\text{find } \mathbf{S}\in\mathbb{C}^{\mathrm{MP}\times\mathrm{MP}} \quad \text{such that} \begin{cases} \operatorname{rank}(\mathbf{S})=r \\ \|\mathcal{A}(\mathbf{S})-\hat{\mathbf{S}}_{pp}^{m}\|_F\le\epsilon \\ \|\boldsymbol{\Psi}\mathbf{S}\boldsymbol{\Psi}^{*}-\mathbf{S}\|_F\le\varepsilon \\ \mathbf{S}^{*}=\mathbf{S}\succcurlyeq 0. \end{cases} \tag{10}$$

A full spectral matrix $\mathbf{S}$ is sought under four constraints which are explained separately hereafter:

(1) *Low rank spectral matrix*: One wants to find matrix $\mathbf{S}$ with given rank r, which estimates the low rank $\mathbf{S}_{pp}^{L}=\mathbf{H}\mathbf{S}_{cc}\mathbf{H}^{*}$ matrix in Eq. (9). This is explained in Section 3.1.
(2) *System equation*: The system equation $\mathcal{A}(\mathbf{S})+\mathbf{E}=\hat{\mathbf{S}}_{pp}^{m}$ represents the data fitting relation, where the unknown spectral matrix $\mathbf{S}$ to be searched is linked to the partial measurements $\hat{\mathbf{S}}_{pp}^{m}$ by the sampling operator $\mathcal{A}:\mathbb{C}^{\mathrm{MP}\times\mathrm{MP}}\to\mathbb{C}^{\mathrm{MP}\times\mathrm{MP}}$ that extracts the elements from diagonal blocks, and where $\mathbf{E}$ is composed of estimation and measurement errors. This system equation is imposed as a constraint $\|\mathcal{A}(\mathbf{S})-\hat{\mathbf{S}}_{pp}^{m}\|_F\le\epsilon$ in the model (10), where the difference between $\mathcal{A}(\mathbf{S})$ and $\hat{\mathbf{S}}_{pp}^{m}$ in Frobenius norm is less than a given tolerance ϵ.
(3) *Spatial continuity of the acoustic field*: In order to ensure spatial continuity of the acoustic field, the information on microphone positions must be encoded in the spectral matrix: $\|\boldsymbol{\Psi}\mathbf{S}\boldsymbol{\Psi}^{*}-\mathbf{S}\|_F\le\varepsilon$, where $\boldsymbol{\Psi}$ is a projection basis; this is explained in Section 3.2.
(4) *Hermitian property and positive semi-definiteness of the spectral matrix*: $\mathbf{S}^{*}=\mathbf{S}\succcurlyeq 0$, where $\succcurlyeq$ denotes positive semi-definite. The Hermitian property is an inherent characteristic of spectral matrices, as well as the fact that its eigenvalues are non-negative.

It is noted that the third and fourth constraints make the problem at hand rather different from other matrix completion problems found in the literature [24,25], which is the reason why it is referred to as “structured low rank” model. The low rank prior and spatial continuity of the acoustic field are explained in the following subsections.

3.1. Low rank spectral matrix

3.1.1. Low rank model background: from sparse representation to low rank model

With the explosion of massive amounts of high-dimensional data in science and engineering, new tools are required to extract intrinsic structure in high-dimensional data so as to alleviate the curse of dimensionality [26,27]. Sparse

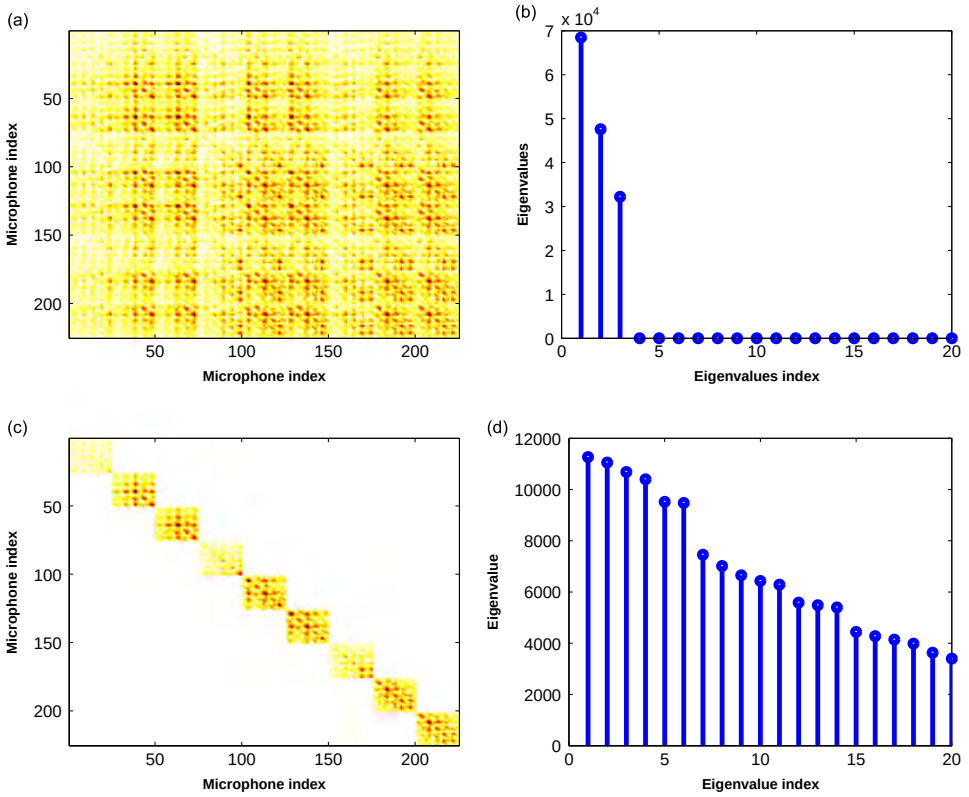

Fig. 4. (a) Full spectral matrix $\mathbf{S}_{pp}^{L}$ and (b) its eigenvalue distribution, (c) measured spectral matrix $\hat{\mathbf{S}}_{pp}^{m}$ and (d) its eigenvalue distribution.

representation is a rapidly evolving field of research [28], with several applications in acoustics [11,12,29,30]. A structured signal can be decomposed with a few elements in an over-complete dictionary that reflects the low dimensional structure of the original signal. A "low rank model" can be seen as an extension of sparse representation: the low rank property of a matrix is a natural generalization of the sparsity of a vector [31,32], which is defined as a matrix with only a few non-zero singular values. The low rank model assumes that the information of interest has a compact structure embedded in a high dimensional space [27,33].

3.1.2. *Low rank in acoustics*

In acoustics, the rank of the spectral matrix has its specific physical implications. The rank of $\mathbf{S}_{pp}^{L}$ measures the stochastic model complexity of the acoustic field, that is the number of latent variables (uncorrelated sources) required to produce the pressure measurement $\mathbf{p}$ [34]. Furthermore, the rank of the spectral matrix indicates the correlation of the acoustical field. For instance, a rank-one spectral matrix corresponds to a fully coherent field, whereas a spectral matrix with full rank corresponds to a diffuse field in general. When the spectral matrix $\mathbf{S}_{pp}^{L}$ is low rank, there exists a hidden low dimension structure in the spectral matrix: Fig. 4 shows an example of a spectral matrix $\mathbf{S}_{pp}^{L}$ under a setup with 3 sources. The full spectral matrix $\mathbf{S}_{pp}^{L}$ is shown in Fig. 4(a) with corresponding eigenvalues in Fig. 4(b); all the energies are concentrated in the first 3 eigenvalues which indicate the number of sources; the spectral matrix $\hat{\mathbf{S}}_{pp}^{m}$ from sequential measurements is shown in Fig. 4(c) which is made only of diagonal blocks with corresponding eigenvalues in Fig. 4(d), and the energy is nearly scattered over the whole eigenvalues axis.

3.1.3. *A naive solution*

The low rank assumption can be seen as an a priori information to be imposed to solve the inverse problem from a Bayesian perspective [35,36,33]. Thus, it shrinks the space of solutions by adding a constraint. Accordingly, the spectral matrix completion problem can be formulated as fitting a low rank spectral matrix $\mathbf{S}$ to the partial measurements $\hat{\mathbf{S}}_{pp}^{m}$, i.e.

$$\text{find } \mathbf{S} \in \mathbb{C}^{\mathrm{MP}\times\mathrm{MP}} \quad \text{such that} \begin{cases} \operatorname{rank}(\mathbf{S}) = r \\ \| \mathcal{A}(\mathbf{S}) - \hat{\mathbf{S}}_{pp}^{m} \|_F \le \epsilon \\ \mathbf{S}^{*} = \mathbf{S} \ge 0. \end{cases} \tag{11}$$

Problem (11) can be solved by Alternating Projection [25] or other methods [24,37] under some conditions on the number and the distribution of the elements in the matrix, the coherence of the eigenvectors, etc. Unfortunately, it has no unique

solution for block diagonal matrices of the type $\hat{\mathbf{S}}_{pp}^{m}$. An example is given here to illustrate this fact (see [24] for a proof). Assume that the measured matrix $\hat{\mathbf{S}}_{pp}^{m}$ is a 2-by-2 complex Hermitian matrix $\begin{pmatrix} 1 & a^{-1} \\ a & 1 \end{pmatrix}$, where $a = \|a\| e^{j\varphi}$ is an unknown complex element and the diagonal elements are known measurements without error. By definition the objective matrix $\mathbf{S}$ is a rank-1 matrix and it is straightforward to find that $\|a\| e^{j\varphi} = \|a\|^{-1} e^{-j\varphi}$ as a result of Hermitian symmetry. Therefore, the solution of Eq. (11) is non-unique since it can be written as $\{a: \|a\| = 1, \forall \varphi\}$. Thus, another constraint is needed as explained in the next section.

3.2. Enforcing spatial continuity of the acoustic field

The spectral matrix $\mathbf{S}_{pp}^{L}$ reflects the correlation between the Fourier coefficients of the measurements, however, it does not contain information on the position of the microphones. For example, two adjacent columns in the spectral matrix must become equal if the corresponding microphones are moved close to each other due to the spatial continuity of the acoustic field; accordingly, this information must be incorporated in the current problem. In this work, the spatial position of the microphones is encoded in the matrix completion problem by introducing an additional constraint. It is assumed that the measured pressure $\mathbf{p}$ with size MP × 1 can be decomposed onto a reduced-dimension spatial basis $\mathbf{\Phi} \in \mathbb{C}^{\mathrm{MP} \times K_p}$ ($K_p < \mathrm{MP}$) with coefficients $\boldsymbol{\vartheta} \in \mathbb{C}^{K_p \times 1}$ as follows:

$$\mathbf{p} = \sum_{i=1}^{K_p} \phi_i(\mathbf{r}) \vartheta_i = \mathbf{\Phi} \boldsymbol{\vartheta}, \tag{12}$$

where $\phi_i(\mathbf{r})$ is the i-th column of matrix $\mathbf{\Phi}$ and ϑ_i is the i-th entry of vector $\boldsymbol{\vartheta}$. In this paper, the Fourier basis is chosen, meaning that the acoustical field is decomposed as a sum of "acoustical modes" [38]. Therefore, a spatial structure is encoded. The coefficients $\boldsymbol{\vartheta}$ are related to the measurements as:

$$\boldsymbol{\vartheta} = \mathbf{\Phi}^{\dagger} \mathbf{p}, \tag{13}$$

where † denotes the pseudoinverse of a matrix as a result of $\mathbf{\Phi}$ not being generally invertible. Then the smoothed pressure $\tilde{\mathbf{p}}$ can be represented as [7]

$$\tilde{\mathbf{p}} = \mathbf{\Phi} \mathbf{\Phi}^{\dagger} \mathbf{p} = \mathbf{\Psi} \mathbf{p}, \tag{14}$$

where $\mathbf{\Psi} = \mathbf{\Phi} \mathbf{\Phi}^{\dagger}$ is defined as a projection operator. Now, let $\mathbf{S} \doteq \mathbb{E}\{\mathbf{p}\mathbf{p}^*\}$ and $\tilde{\mathbf{S}} \doteq \mathbb{E}\{\tilde{\mathbf{p}}\tilde{\mathbf{p}}^*\}$. Therefore,

$$\tilde{\mathbf{S}} = \mathbf{\Psi} \mathbf{S} \mathbf{\Psi}^*. \tag{15}$$

Eq. (15) may be rewritten as $\|\mathbf{\Psi}\mathbf{S}\mathbf{\Psi}^* - \mathbf{S}\|_F \leq \varepsilon$ where ε is the representation error between $\mathbf{\Psi}\mathbf{S}\mathbf{\Psi}^*$ and $\mathbf{S}$ owing to the $\mathbf{\Phi}$ truncation. It is important that $\mathbf{\Psi}$ imposes a specific structure that encodes the information on microphone positions into the matrix $\mathbf{S}$. This can be seen as another constraint to be added to Eq. (11), thus leading to Eq. (10).

The orthogonal projection operator $\mathbf{\Psi}$ can be further explained by decomposing it as $\mathbf{U}\begin{pmatrix} \mathbf{I}_{K_p} & 0 \\ 0 & 0 \end{pmatrix}\mathbf{U}^*$, where $\mathbf{U}\mathbf{U}^* = \mathbf{I}$, $\mathbf{I}_{K_p}$ is the identity matrix with n elements, and $\mathbf{U}$ is the modal matrix in the eigenvalue decomposition (EVD) of $\mathbf{\Phi}$. Then Eq. (14) reads

$$\tilde{\mathbf{p}} = \mathbf{\Psi} \mathbf{p} = \sum_{i=1}^{K_p} (\mathbf{p}^* \mathbf{u}_i)^* \mathbf{u}_i. \tag{16}$$

This means that only the $\mathbf{p}^*\mathbf{u}_i$, $i = 1 \ldots K_p$, part corresponding to the eigenvalues of $\mathbf{\Psi}$ equal to one are kept. It is important to emphasize that the role of the orthogonal projection operator $\mathbf{\Psi}$ is to smooth the spectral matrix and to ensure the spatial continuity of the acoustical field.

3.2.1. Spatial basis construction

The basis functions of the Fourier basis are $\Phi(x, y) = e^{i(k_x x + k_y y)}$ [1] where x, y are the coordinates of the microphones in the array and k_x and k_y the wavenumbers along the x and y directions respectively (note that the Fourier basis might be non-regularly sampled). The wavenumbers are discretized as $k_x^n = n\Delta k_x$ (resp. $k_y^n = n\Delta k_y$), $n = -N, \ldots, N$ where the maximum spatial frequency $k_{\max} = N\Delta k_x = \frac{\pi}{\Delta x}$ (resp. $N\Delta k_y = \frac{\pi}{\Delta y}$) is related to the minimum spatial resolution Δx (resp. Δy) and $\Delta k_x = \frac{2\pi}{L_x}$ (resp. $\Delta k_y = \frac{2\pi}{L_y}$) is the spatial resolution related to the aperture length L_x (resp. L_y). The dimension of Φ is MP × K_p ($K_p < \mathrm{MP}$): MP is the total number of microphones (number of microphones in the array times the number of sequential measurements) virtually used in sequential measurements, where K_p is determined by choosing the minimum spatial resolution appropriately. Guidelines as how to choose the minimum spatial resolution is discussed in Section 5.1.1.

4. Cyclic Projection

This section now discusses as how to solve problem (10) by Cyclic Projection.

4.1. From alternating projection to Cyclic Projection

Alternating Projection is a method to find a point at the intersection of two closed convex sets by using a sequence of projections from one set to the other [25]. The iteration procedure can be defined sequentially as follows. Suppose that $\mathbf{C}$ and $\mathbf{D}$ are two closed convex sets (every point on the line segment connecting every pair of points within the set) in $\mathbb{R}^N$, and define $P_{\mathbf{C}}$ and $P_{\mathbf{D}}$ the projections on $\mathbf{C}$ and $\mathbf{D}$ respectively. The algorithm starts with an arbitrary value $x_k \in \mathbf{C}$ and then generates the iteration sequence:

$$\begin{cases} y_k = P_{\mathbf{D}}(x_k) \\ x_{k+1} = P_{\mathbf{C}}(y_k), \quad k = 0, 1, 2\ldots \end{cases}$$

where $x_k \in \mathbf{C}$ and $y_k \in \mathbf{D}$. In other words, $x_k \in \mathbf{C}$ is projected onto $y_k \in \mathbf{D}$ first and second $y_k \in \mathbf{D}$ is projected back onto set $\mathbf{C}$ and so forth. One of the simplest situations is when $\mathbf{C}$ and $\mathbf{D}$ are closed convex sets and $\mathbf{C} \bigcap \mathbf{D} \neq \varnothing$ (the intersection is non-empty), in which case the convergence rate of the iterations is proven to be linear [39]. When $\mathbf{C} \bigcap \mathbf{D} = \varnothing$ (the intersection is empty), alternating projections yields a pair of points in $\mathbf{C}$ and $\mathbf{D}$ that have minimum distance $\| x^\star - y^\star \|_2 = \mathrm{dist}(\mathbf{C}, \mathbf{D})$, where x_k converges to $x^\star$ in $\mathbf{C}$ and y_k converges to $y^\star$ in $\mathbf{D}$ [40]. When $\mathbf{C}$ or $\mathbf{D}$ is not a convex set, alternating projection has no convergence proof in general (despite local linear convergence when the strong regularity condition holds [41]), yet it is still a popular heuristic to solve the optimization problem. Cyclic Projection (CP) is an extension of the basic alternating projection algorithm that generalizes the number of sets to more than 2. Specifically, it can find a point at the intersection of $k > 2$ sets by projecting alternatively onto $\mathbf{C}_1$, then $\mathbf{C}_2, \ldots$, and then $\mathbf{C}_k$. In order to use CP to solve the current problem in this paper, the sets and the projection operators should be defined separately, which is the objective of the next section.

4.2. Predefined sets and operators

4.2.1. Sampling operator

The sampling operator and its corresponding set are easily defined according to the specific structure of the spectral matrix resulting from the sequential measurements mode. Sequential measurements produce a block diagonal spectral matrix, thus $\mathbf{C}_1$ is defined as an affine set in the set of $n \times n$ Hermitian matrices $\mathbf{S}^n$ with specified block entries and the sampling operator $P_{\mathbf{C}_1}$ is defined such that

$$\mathbf{B} = P_{\mathbf{C}_1}\{\mathbf{A}\} \quad \text{with } \mathbf{B}_{ij} = \begin{cases} [\hat{\mathbf{S}}_{pp}^m]_{ij} & ij \in \boldsymbol{\Upsilon} \\ [\mathbf{A}]_{ij} & ij \notin \boldsymbol{\Upsilon}, \end{cases}$$

where $[]_{ij}$ denotes the (i, j) element of a matrix and $\boldsymbol{\Upsilon}$ denotes the positions of fixed block diagonal entries. The sampling operator forces the actual measurements to be kept unchanged in each iteration step.

4.2.2. Eigenvalue truncation operator

$\mathbf{C}_2 = \mathbf{S}_+^n$ is defined as the set of Hermitian positive semidefinite $n \times n$ matrices with reduced rank. Note that this is a non-convex set [42] and the corresponding projection $\mathbf{B} = P_{\mathbf{C}_2}\{\mathbf{A}\}$ is defined as

$$\begin{cases} \mathbf{A} = \sum_{i=1}^n \lambda_i \mathbf{u}_i \mathbf{u}_i^* = \sum_{i=1}^r \lambda_i \mathbf{u}_i \mathbf{u}_i^* + \sum_{i=r+1}^n \lambda_i \mathbf{u}_i \mathbf{u}_i^* \\ \mathbf{B} = \sum_{i=1}^r \lambda_i \mathbf{u}_i \mathbf{u}_i^*. \end{cases}$$

First, matrix $\mathbf{A}$ is factorized into n eigen-elements, then only the first r largest eigenvalues and their corresponding eigenvectors are preserved. The eigenvalue truncation operator can be recognized as a hard threshold [43,44] to fulfill the low rank matrix approximation of the spectral matrix.

4.2.3. Spatial continuity enforcing operator

The last closed convex set is defined as $\mathbf{C}_3 = \{\mathbf{B} \in \mathbb{C}^{\mathrm{MP} \times \mathrm{MP}} : \mathbf{B} = \boldsymbol{\Psi}\mathbf{A}\boldsymbol{\Psi}^*, \forall \mathbf{A} = \mathbf{A}^*\}$. The corresponding projection $P_{\mathbf{C}_3}\{\mathbf{A}\}$ denotes an operator that maps the elements $\{\mathbf{A}\}$ onto set $\mathbf{C}_3$ by $\mathbf{B} = \boldsymbol{\Psi}\mathbf{A}\boldsymbol{\Psi}^*$. The introduction of this operator is to endow the spectral matrix with information on spatial positions of the microphones, meanwhile enforcing the spatial continuity of acoustic field.

4.3. Cyclic Projection

The solution of problem (10) is assumed to be located at the intersection of the three sets $\mathbf{C}_1$, $\mathbf{C}_2$, and $\mathbf{C}_3$, and is solved by CP. First, the initial value $\hat{\mathbf{S}}^{\{0\}}$ is given (for example, a zero matrix); in each step, the measurements are assigned by projecting $\hat{\mathbf{S}}^{\{k\}}$ onto set $\mathbf{C}_1$ to produce $\tilde{\mathbf{S}}^{\{k\}}$. Subsequently, matrix $\tilde{\mathbf{S}}^{\{k\}}$ is decomposed into eigen-elements, and a low rank approximation is proceeded by truncation: this projects $\tilde{\mathbf{S}}^{\{k\}}$ onto set $\mathbf{C}_2$ to produce $\check{\mathbf{S}}^{\{k\}}$. Last, spatial continuity is enforced by projecting $\check{\mathbf{S}}^{\{k\}}$ onto set $\mathbf{C}_3$ to produce $\hat{\mathbf{S}}^{\{k+1\}}$. In CP, the order of the cycles is not important, thus the procedure that is described here is only one possibility. For instance, it could also be written as $\mathbf{C}_3 \rightarrow \mathbf{C}_2 \rightarrow \mathbf{C}_1$ and so on. The iteration will be

stopped when $\frac{\|[\hat{\mathbf{S}}^{m}]_{ij}-[\hat{\mathbf{S}}^{(k)}]_{ij}\|_F}{\|[\hat{\mathbf{S}}^{m}]_{ij}\|_F} \le \mathrm{SC},\ ij \in \Upsilon$ (SC is a constant value that is chosen by the user) after projecting onto $\mathbf{C}_1$ and $\mathbf{C}_2$, then forcing the final solution to be low rank. The proposed CP has only three parameters to tune: the first one is the maximum iteration number $M_{\max}$, the second one is the stopping criteria SC which usually depends on the noise level, and the third one is the rank r which reflects the number of uncorrelated sources in the field. In practice, the rank can be estimated independently from each array position [34,45]. The maximum number of iterations should be large enough to make sure that the algorithm reaches convergence in any case as characterized by a small stopping criterion.

Algorithm 1. Cyclic Projection (CP)

1: Starts with $\hat{\mathbf{S}}^{(0)} \in \mathbb{C}^{\mathrm{MP}\times\mathrm{MP}}$.
2: **While** Iteration number $< M_{\max}$ **do**
3: $\hat{\mathbf{S}}^{(k)} = P_{\mathbf{C}_1}(\hat{\mathbf{S}}^{(k)})$.
(Keep the measurements unchanged in diagonal blocks: project from set $\mathbf{C}_3$ onto set $\mathbf{C}_1$)
4: $\hat{\mathbf{S}}^{(k)} = \sum_{i=1}^{n} \sigma_i^2 \mathbf{u}_i \mathbf{u}_i^*$.
5: $\hat{\mathbf{S}}^{(k)} = P_{\mathbf{C}_2}(\hat{\mathbf{S}}^{(k)}) = \sum_{i=1}^{r} \sigma_i^2 \mathbf{u}_i \mathbf{u}_i^*$.
(Eigenvalues truncation: project from set $\mathbf{C}_1$ onto set $\mathbf{C}_2$)
6: **If** Stopping criteria $\le$ SC, **break**
7: $\hat{\mathbf{S}}^{(k+1)} = P_{\mathbf{C}_3}(\check{\mathbf{S}}^{(k)}) = \boldsymbol{\Psi}\check{\mathbf{S}}^{(k)}\boldsymbol{\Psi}^*$.
(Enforcing spatial continuity: project from set $\mathbf{C}_2$ onto set $\mathbf{C}_3$)
8: go to step 3.

4.4. Error analysis

Four kinds of errors are considered: (1) background noise, (2) estimation errors of the spectral matrix, (3) model errors (for example the calibration error of the microphones, the position error of the array, etc.), and (4) representation errors caused by the smoothing operator in Eq. (14). Operator $P_{\mathbf{C}_1}$ brings about errors (1), (2), operator $P_{\mathbf{C}_2}$ error (1), and operator $P_{\mathbf{C}_3}$ errors (3), (4). The structured low-rank completion problem (10) can be reformulated as the projection representation with error terms (ξ, ϵ, ε):

$$\text{find } \mathbf{S} \in \mathbb{C}^{\mathrm{MP}\times\mathrm{MP}} \quad \text{such that} \begin{cases} \|P_{\mathbf{C}_2}(\mathbf{S})-\mathbf{S}\|_F \le \xi \text{ (error (1))} \\ \|P_{\mathbf{C}_1}(\mathbf{S})-\mathbf{S}\|_F \le \epsilon \text{ (errors (1), (2))} \\ \|P_{\mathbf{C}_3}(\mathbf{S})-\mathbf{S}\|_F \le \varepsilon \text{ (errors (3), (4)).} \end{cases} \tag{17}$$

This projection representation with error terms may provide more flexibility to apply the CP algorithm in practice. For example, when the errors (1), (2) are too large and errors (3), (4) are acceptable, then the user may choose the stopping criteria according to the constraint $\|P_{\mathbf{C}_3}(\mathbf{S}^{(k)})-\mathbf{S}^{(k+1)}\|_F \le \varepsilon$.

5. Simulation and parameter analysis

In this section, several simulations are run to test the sequential measurements algorithms with and without references under various scenarios. Three point sources with equivalent unit magnitudes located separately at $(0.2701, -0.0084)$, $(-0.1613, 0.2348)$, and $(0.0641, 0.1573)$ (m) are simulated to generate the acoustic field. In order to compare the errors of sound source reconstruction hereafter, the source plane is discretized uniformly by a 41×41 grid with distance 0.025 m, length 1 m and width 1 m, and these three point sources are expanded in a B-spline basis [23] to produce a smoothed velocity distribution; an example of simulated sources is given in Fig. 6. The air mass density is 1.2 kg/m^3 and the sound velocity is 341 m/s. The measurement plane is located at 0.1 m away from the source plane: the microphones are uniformly distributed with spacing 0.1 m in a square array with side length 0.4 m; the total number of microphones in the array is 25. Complex Gaussian noise is added to 100 snapshots to produce the measured pressures (in frequency domain), and the spectral matrices of the simultaneous measurements (full matrix) and sequential measurements are separately estimated. All the simulations given in this paper are based upon five setups.

- *Setup* 1: *simulation of sequential measurements without reference* (*see* Fig. 5(*b*)). The prototype array is shifted 9 times sequentially at positions $(-0.16, -0.16)$, $(-0.16, 0.08)$, $(-0.16, 0.16)$, $(0.08, -0.16)$, $(0.08, 0.08)$, $(0.08, 0.16)$, $(0.16, -0.16)$, $(0.16, 0.08)$, and $(0.16, 0.16)$ (m). This setup is mainly used to verify and test the CP algorithm under diverse choices of the basis and SNR value in the case without reference.
- *Setup* 2: *simulation of sequential measurements with references*. The sequential measurements are carried out as in Setup 1, but different numbers of references are considered:
  - 4 references (see Fig. 5(c)) at positions $(-0.20, 0.25)$, $(-0.20, 0.15)$, $(-0.20, 0.05)$, and $(-0.20, -0.05)$;
  - 3 references at positions $(-0.20, 0.25)$, $(-0.20, 0.15)$, and $(-0.20, 0.05)$;

- 2 references at positions $(-0.20, 0.25)$ and $(-0.20, 0.15)$;
- 1 reference at position $(-0.20, 0.25)$ (m).

A performance comparison with the classic method [17] is provided by using this setup.

Setups 3–5 are used to investigate the algorithm performance with respect to different relative distances between consecutive measurements. The positions of references are as in Setup 2.

- *Setup* 3: *simulation of sequential measurements without and with references* (*see* Fig. 5(*d*)): The prototype array is shifted 9 times sequentially at positions $(-0.42, -0.42)$, $(-0.42, 0.08)$, $(-0.42, 0.43)$, $(0.08, -0.42)$, $(0.08, 0.08)$, $(0.08, 0.43)$, $(0.43, -0.42)$, $(0.43, 0.08)$, and $(0.43, 0.43)$ (m).

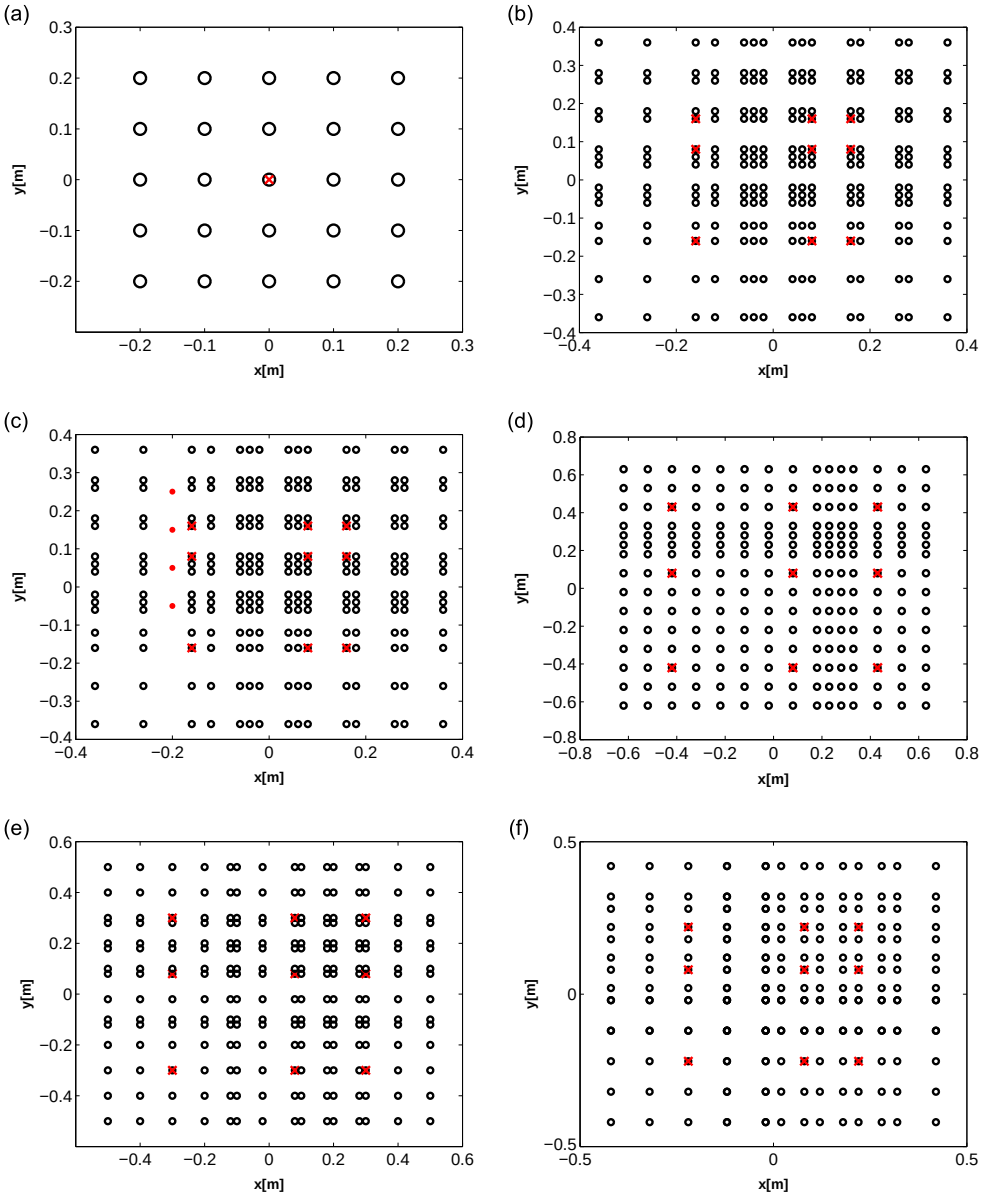

Fig. 5. Simulation setups: (a) a prototype array with 25 microphones (center microphone position is marked with red cross), (b) Setup 1, (c) Setup 2, (d) Setup 3 (the reference microphones are marked with red point), (e) Setup 4, and (f) Setup 5 (only the case without reference is shown in Setups 3–5, and center microphone position in prototype array is shifted 9 times sequentially which is marked with red crosses in Setups 1–5). (For interpretation of the references to color in this figure caption, the reader is referred to the web version of this paper.)

- *Setup* 4: *simulation of sequential measurements without and with references* (*see Fig. 5*(*e*)): The prototype array is shifted 9 times sequentially at positions $(-0.3, -0.3)$, $(-0.3, 0.08)$, $(-0.3, 0.3)$, $(0.08, -0.3)$, $(0.08, 0.08)$, $(0.08, 0.3)$, $(0.3, -0.3)$, $(0.3, 0.08)$, and $(0.3, 0.3)$ (m).
- *Setup* 5: *simulation of sequential measurements without and with references* (see Fig. 5(f)): the prototype array is moved 9 times sequentially at positions $(-0.22, -0.22)$, $(-0.22, 0.08)$, $(-0.22, 0.22)$, $(0.08, -0.22)$, $(0.08, 0.08)$, $(0.08, 0.22)$, $(0.22, -0.22)$, $(0.22, 0.08)$, and $(0.22, 0.22)$ (m).

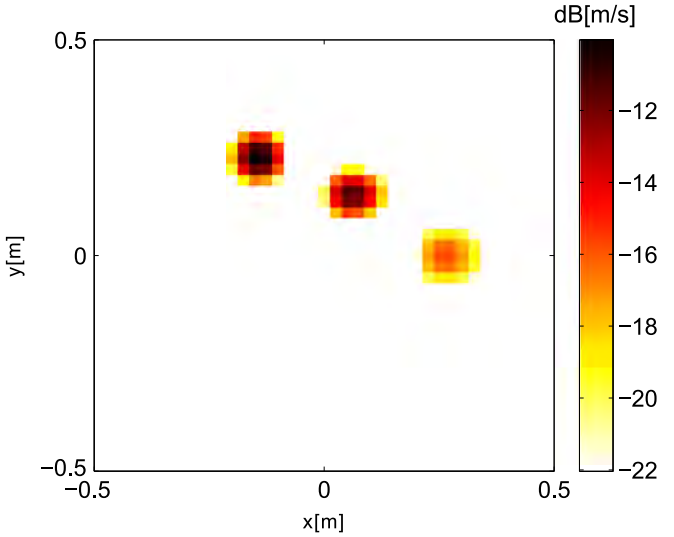

Fig. 6. Velocity distribution of simulated sources.

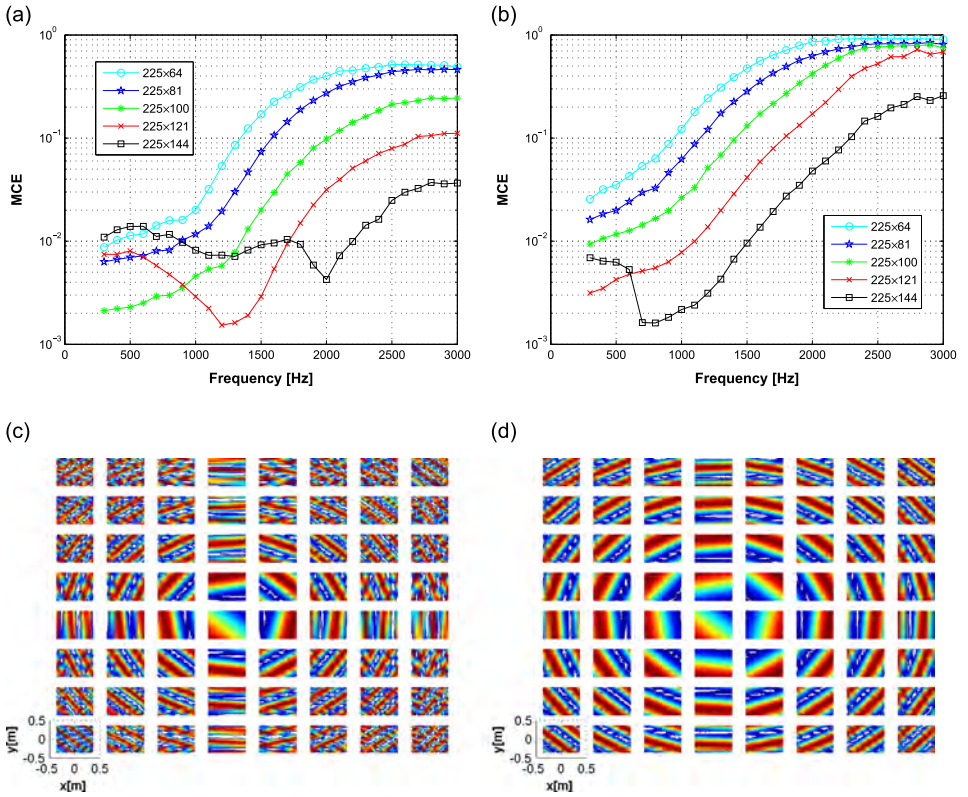

Fig. 7. Sequential measurements with different spatial bases: spectral matrix completion errors (MCE) with (a) $L_x = L_y = 1$ m and (b) $L_x = L_y = 2$ m (spatial bases are indicated by their dimensions 225×64, 225×81, 225×100, 225×121, 225×144); display of the spatial bases (real part) in the case (c) 64×64 Fourier basis with parameters $L_x = L_y = 1$ m and $\Delta x = \Delta y = 0.12$ m and (d) 64×64 Fourier basis with parameters $L_x = L_y = 2$ m and $\Delta x = \Delta y = 0.24$ m.

The parameters of the CP algorithm are chosen as follows: maximum iteration numbers $M_{\max}=6000$, stopping criteria $\mathrm{SC}=10^{-3}$, rank $r=3$. Two figures of merit are considered: (1) the spectral matrix completion error (MCE) calculated as

$$\mathrm{MCE}=\frac{\|\mathbf{S}_{pp}^{\{\mathrm{sim}\}}-\mathbf{S}_{pp}^{\{\mathrm{com}\}}\|_F}{\|\mathbf{S}_{pp}^{\{\mathrm{sim}\}}\|_F}, \tag{18}$$

where $\mathbf{S}_{pp}^{\{\mathrm{sim}\}}$ is the simulated spectral matrix and $\mathbf{S}_{pp}^{\{\mathrm{com}\}}$ is the completed spectral matrix and (2) the sound source reconstruction error (ARE) calculated as

$$\mathrm{ARE}=\frac{\|\mathbf{S}^{\{\mathrm{sim}\}}-\mathbf{S}^{\{\mathrm{rec}\}}\|_F}{\|\mathbf{S}^{\{\mathrm{sim}\}}\|_F}, \tag{19}$$

where $\mathbf{S}^{\{\mathrm{sim}\}}$ is the simulated source and $\mathbf{S}^{\{\mathrm{rec}\}}$ is the reconstructed one using the method of Ref. [23] based on the completed spectral matrix.

5.1. Sequential measurements without reference

5.1.1. Choice of the spatial basis

First, the spectral matrix completion results are investigated with the Fourier basis in Setup 1 and the SNR is fixed to 60 dB. The first group of bases is constructed with $L_x=L_y=1$ m and Δx ($=\Delta y$) is set to 0.12, 0.11, 0.10, 0.09, and 0.08 (m), resulting in dimensions of 225×64, 225×81, 225×100, 225×121, 225×144 respectively. The corresponding MCE curves up to 3 kHz are shown in Fig. 7(a). When more and more basis components are introduced up to a certain point (about 144 components) corresponding to $\Delta x=0.08$ m, the MCE decreases. However, this increase cannot be unlimited (the guideline and the safe bound to construct the basis will be explained later in this section). The second group of spatial bases is constructed with a measurement aperture $L_x=L_y=2$ m and Δx is set to 0.24, 0.22, 0.20, 0.18, and 0.16 (m), resulting in basis dimensions of 225×64, 225×81, 225×100, 225×121, 225×144 respectively. The corresponding MCE curves are shown in Fig. 7(b). Similar phenomena can be observed as in the previous case, yet the performance is slightly inferior in general: the aperture is chosen large, resulting in fewer high frequency components. This is illustrated in Fig. 7(c), (d), where two bases with identical dimensions 64×64 are compared. Nyquist–Shannon sampling theorem requires that Δx should be at least twice as large as the average distance d_c between the microphones of sequential measurements. Thus, the rule $\Delta x\geq 2d_c$ may be used as the guideline to construct the basis. In the following, the basis is constructed with settings $\Delta x=0.08$ m and $L_x=L_y=1$ m (the corresponding dimension is 225×144), although this choice may not be optimal for all the setups.

5.1.2. Sequential measurements performance analysis with various SNRs

Setup 1 is used here to verify the performance of the spectral matrix completion with respect to various values of the SNR. Fig. 8(a) illustrates the spectral matrix completion results by CP. It is seen that the MCE decreases with the SNR; although the performance of CP is influenced by noise, the MCE in the whole range is less than 0.12. The fact that MCE at 30 dB is lower than at 60 dB in some frequency ranges is caused mainly by the non-optimal choice of the basis function: when the SNR is high (for example SNR=60 dB and 30 dB), the model errors may play a key role in the final results (the basis here may be a better basis for 30 dB than 60 dB, thus 30 dB case has less model errors); when the SNR is relatively low (for example SNR=20 dB and 10 dB), the noise may play a key role in the final results. The completed spectral matrix is further used to reconstruct the sources by back-propagation [23]. Fig. 8(b) illustrates the sound source reconstruction results. It is remarked that the ARE decreases with frequency in general. The spatial aliasing frequency of the prototype array is 1700 Hz, and the ARE by using sequential measurements is far less than 0.01 even at 3000 Hz, which greatly improves the maximum working frequency. It is also observed that the ARE can be quite low even with a relatively high MCE of the

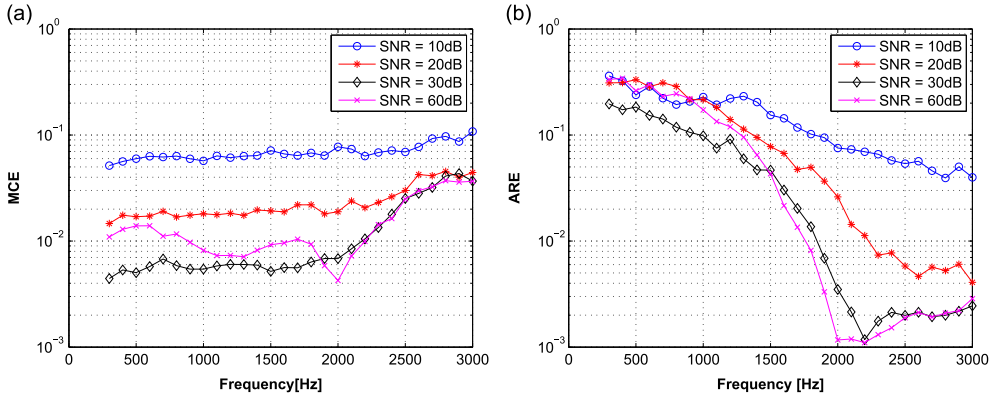

Fig. 8. Sequential measurements without reference (Setup 1): (a) MCE without reference and (b) ARE without reference.

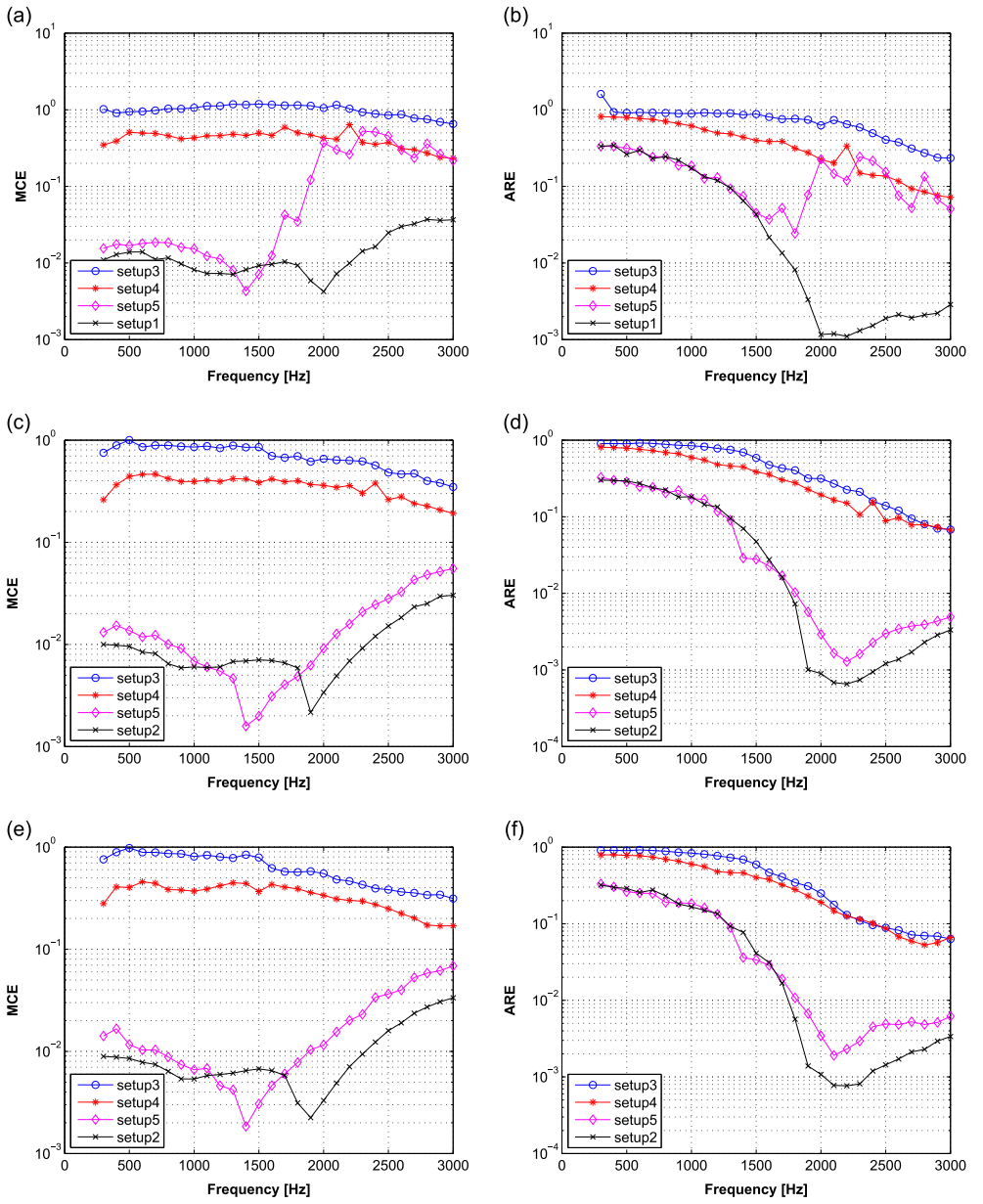

Fig. 9. Reconstruction results (with fixed SNR=60 dB): (a) MCE without reference, (b) ARE without reference. MCE and ARE with one reference (c, d), with two references (e, f).

spectral matrix; take for example 3000 Hz with SNR=10 dB: the MCE is 0.1081, whereas the ARE is 0.0399. This can be explained as a result of regularization (Bayesian regularization [23,46] is used in this paper): the smoothing effect of regularization decreases with the increase of the frequency, thus the reconstruction result is more smoothed at low frequencies and less smoothed at high frequencies.

5.1.3. Sequential measurements with different shift distances

The simulation of this section is based on Setups 1–5 without reference. Fig. 9(a) and (b) shows the MCE and ARE respectively with increasing shift distances. It is seen that the MCE decreases with the shift distance. Small shifts can capture more correlation of the acoustical field; on the contrary, if sequential measurements are carried out far from each other, spatial correlation is lost which renders the spectral matrix harder to complete. Thus, a good spectral matrix completion and sound source reconstruction performance depends on the shifts between sequential measurements.

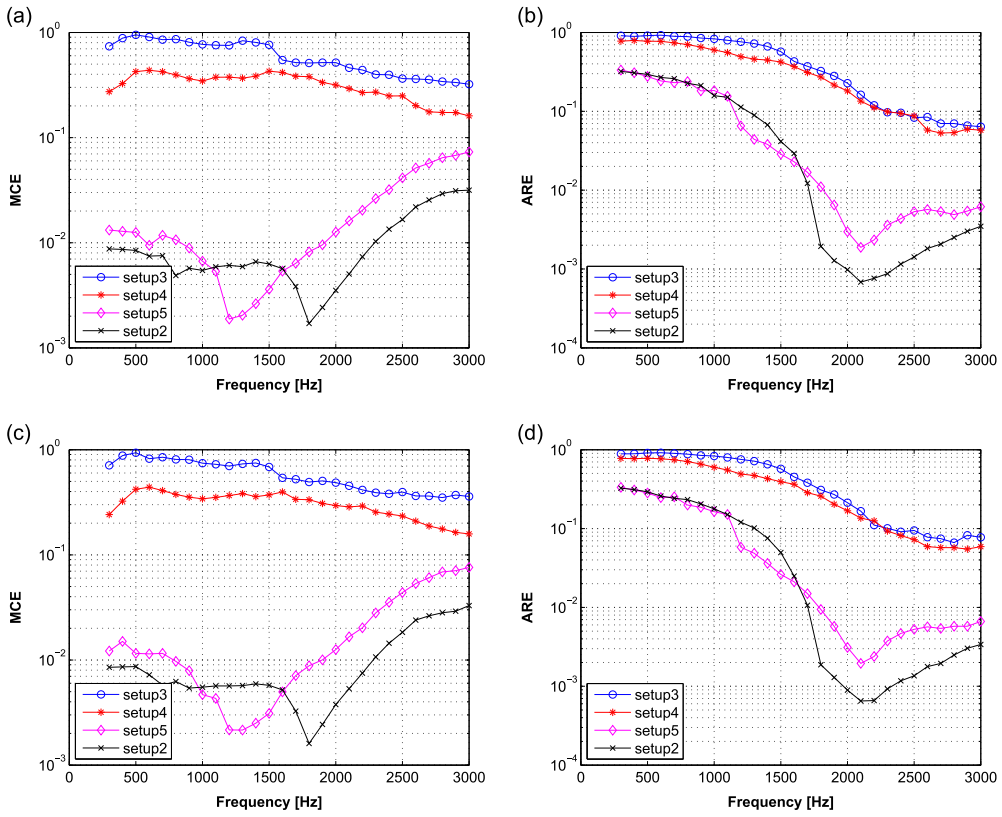

Fig. 10. Reconstruction results (with fixed SNR=60 dB), MCE and ARE with three references (a, b), with four references (c, d).

5.2. *Sequential measurements with references*

In this section, the simulation based on Setups 1–5 with references are firstly investigated. Fig. 9(c) and (d) shows respectively the MCE and ARE in the case of one reference. When the shift is too large, both the MCE and the ARE are affected. Similar facts can be also observed when the number of references is increased in Fig. 9(e), (f) and Fig. 10(a)–(d). Subsequently, CP is also investigated in the case of references under Setup 2 and compared with the classical reference-based method which is optimal in the mean square sense (Mean Square, MS) method [17]. The following cases are identified:

(1) The number of references is larger than the number of sources (i.e. 4 references). When SNR=60 dB, the spectral matrix completion error by MS is far less than by CP (see Fig. 11(a)); when SNR=30 dB, the two methods are comparable (see Fig. 11(c)); CP outperforms MS when SNR $\leq$ 20 dB (see Fig. 12(a) and (c)). When the number of references is greater than or equal to the number of sources in the absence of noise and the MS method is optimal (in the mean square sense); the reference signals then provide enough information on correlation between sequential measurements. However the performance of MS rapidly deteriorates when the level of noise increases.
(2) The number of references is equal to the number of sources (i.e. 3 references). When SNR=60 dB, the spectral matrix completion error by MS is still far less than by CP (see Fig. 11(a)); CP outperforms MS when the SNR $\leq$ 30 dB (see Fig. 11(c), Fig. 12(a) and (c)). Similar conclusion holds as in the previous case, yet with increased sensitivity to noise.
(3) The number of references is less than the number of sources (i.e. 2 references or 1 reference). The MS generally fails to deal with this case, whereas CP still works very well. The MCE is illustrated in Fig. 11(a), (c) and Fig. 12(a), (c).

In conclusion, it is seen that CP returns reasonably with low errors in all investigated scenarios, contrary to MS which rapidly fails when the number of references is insufficient or becomes noisy. It is remarkable that CP achieves more or less the same figure of merit independent of the number of references. The idea of with references is not defending in this paper, one fact is that CP demands less references than necessary which is an advantage as compared with the classic with references method if they are available. As an endnote to this section, it should be highlighted that spectral matrix completion and sound source reconstruction reflect two different problems. ARE in Fig. 11(b), (d) and Fig. 12(b), (d) is not only influenced by the spectral matrix completion errors but also by regularization. The spectral matrix completion errors

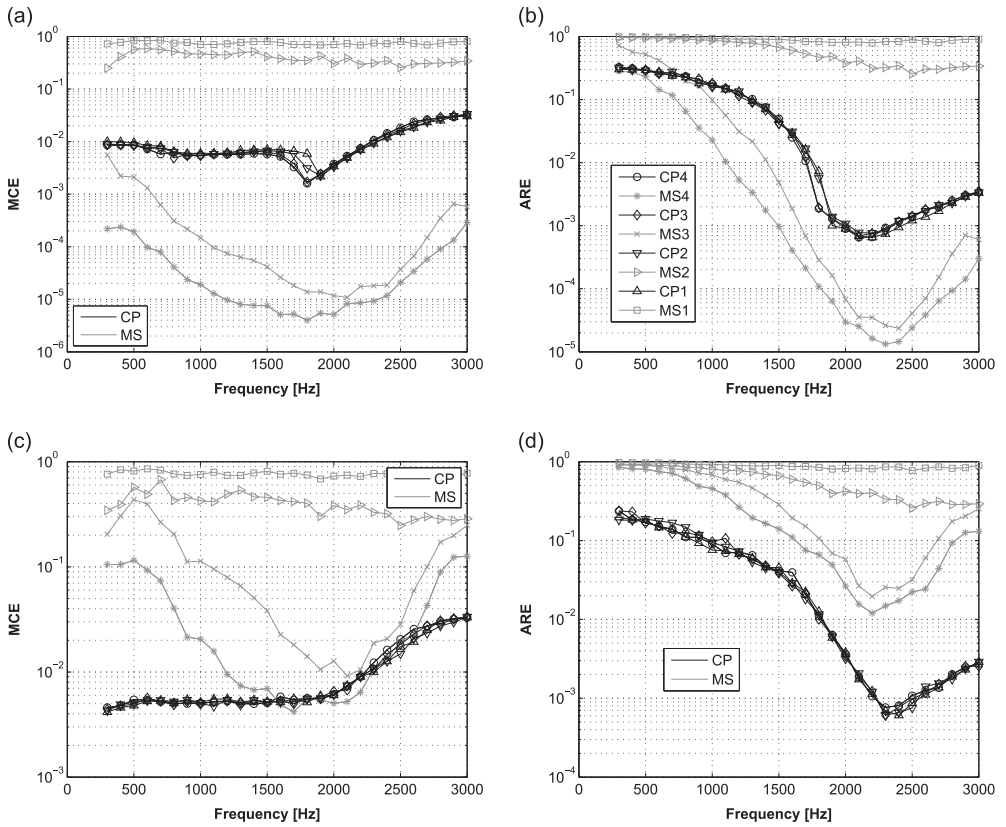

Fig. 11. Reconstruction error with different SNRs and different numbers of references: (a) MCE with SNR=60 dB, (b) ARE with SNR=60 dB, (c) MCE with SNR=30 dB, and (d) ARE with SNR=30 dB. (CP results are shown in black (see the legend in (b)): with 1 reference case by upward-pointing triangle; with 2 references case by downward-pointing triangle; with 3 references case by diamond; with 4 references case by circle. MS results are shown in gray (as the legend in (b)): with 1 reference case by square; with 2 references case by right-pointing triangle; with 3 references case by cross; with 4 references case by asterisk.)

are not always positively correlated with the sound source reconstruction error: ARE could be low with a high MCE due to the effect of regularization.

6. Experimental validation

This section now illustrates the methodology on measurements made in a semi-anechoic chamber. The experimental setup is shown in Fig. 13(a). The sources are 3 Fostex 6301B speakers with 0.1 m diameter and working frequency from 80 Hz to 13 kHz; plates with absorbent material are placed on the ground in order to limit the reflections. A rectangular plane array is used with 5×6 GRAS microphones *PQ* 40 regularly spaced every 0.1 m. A data acquisition system *OROS* with 32 channels associated with the software NVgate is used. The proposed experiment makes use of 3 independent sources. Two are generated with the software NVgate (*OROS*), and the third one is generated externally. The three sources are placed in a plane parallel to the array. The height of the center of the array is 1.17 m. The centers of the two bottom sources are aligned with the center of the array in the initial setup. The center point of the array is considered as the origin of coordinates (0, 0) m. The distance between the source plane and array is 0.73 m and the array is moved at (0, 0), (−0.08, 0), (0.08, 0), (0.08, −0.08), (0, −0.08), (0, 0), (−0.08, −0.08), (−0.08, 0.08), (0, −0.08), and (0.08, 0.08) (m). The sampling frequency is Fs=25.6 kHz. The signals generated for the three sources are independent white noises with frequency bandwidth between 50 Hz and 10 kHz. Two reference signals are acquired directly by two fixed microphones and the third one is taken directly from the signal generator. This provides ideal references with a very high signal to noise ratio. 32 signals (29 microphones and 3 references) are recorded, each with an acquisition time of 10 s. The purpose is to complete a data missing spectral matrix, which can be fed into either near-field or far-field method. The Bayesian focusing method [23] is used for reconstruction. One benefit of this method is to be flexible with respect to the topology of the source surface, the geometry of the array and the type of propagation (near field or far field) by automatically choosing the optimal basis. Note that any existing reconstruction methods can be used and that Bayesian focusing method is just one choice.

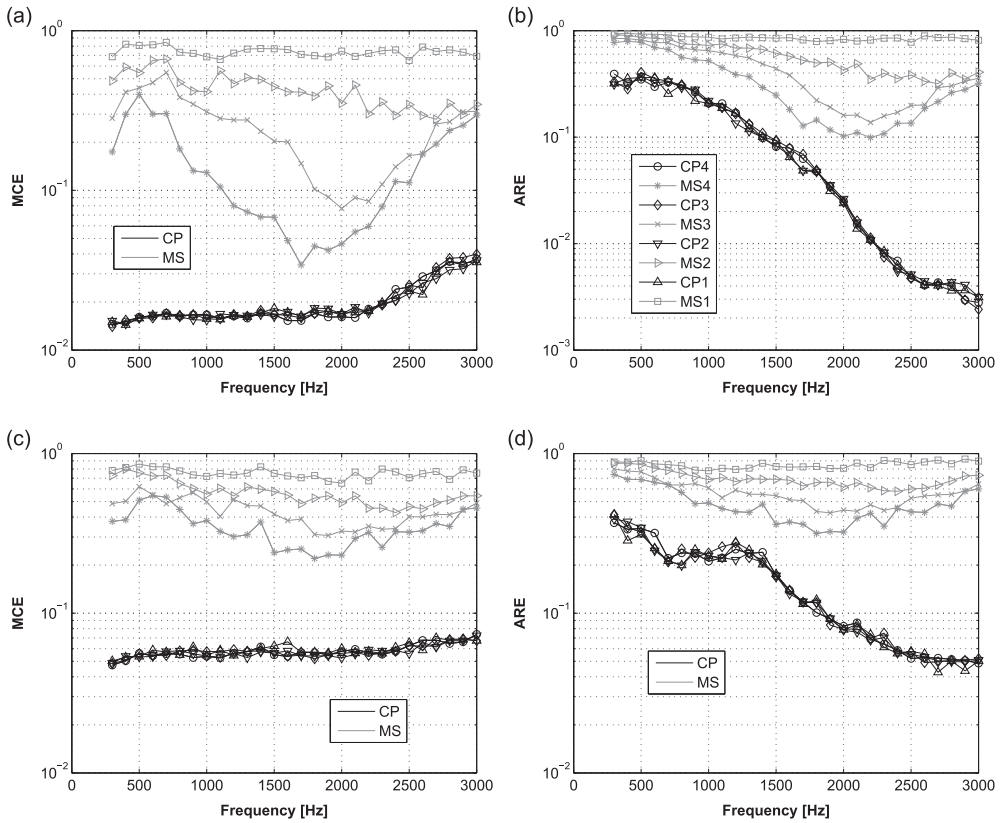

Fig. 12. Reconstruction error with different SNRs: (a) MCE with SNR=20 dB, (b) ARE with SNR=20 dB, (c) MCE with SNR=10 dB, and (d) ARE with SNR=10 dB. (CP results are shown in black (see the legend in (b)): with 1 reference case by upward-pointing triangle; with 2 references case by downward-pointing triangle; with 3 references case by diamond; with 4 references case by circle. MS results are shown in gray (as the legend in (b)): with 1 reference case by square; with 2 references case by right-pointing triangle; with 3 references case by cross; with 4 references case by asterisk.) (For interpretation of the references to color in this figure caption, the reader is referred to the web version of this paper.)

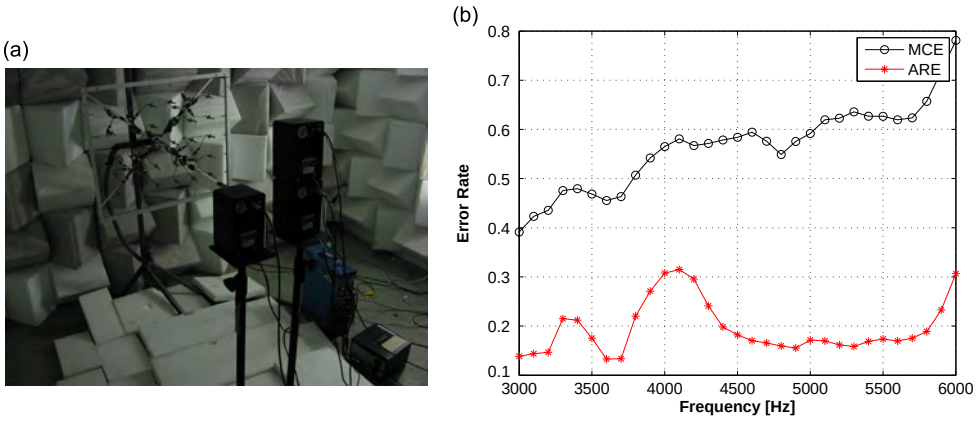

Fig. 13. (a) Experimental setup. (b) MCE and ARE are shown in the same figure and denoted as error rate. MCE is the relative error between the completed spectral matrixes returned by the CP and MS methods, and ARE is the relative error between the reconstructed sources by using the completed spectral matrixes.

The parameter of CP are chosen as follows: maximum iteration number $M_{\max} = 6000$, stopping criteria $SC = 10^{-3}$, rank $r=3$. The Fourier basis is discretized with $\Delta x = \Delta y = 0.1$ m over a surface with length $L_x = 1$ m and width $L_y = 1$ m (the dimension of the basis $\mathbf{\Phi}$ is 225×100). First, the CP and MS methods are used to complete the spectral matrix in the frequency range from 3000 Hz to 6000 Hz with steps of 100 Hz; CP is applied without reference and MS is applied with 3 references. The MS results are used as a point of comparison to validate the CP method, yet with no guarantee that they will return the true values, as shown in the simulation section. The relative completion errors between CP and MS methods

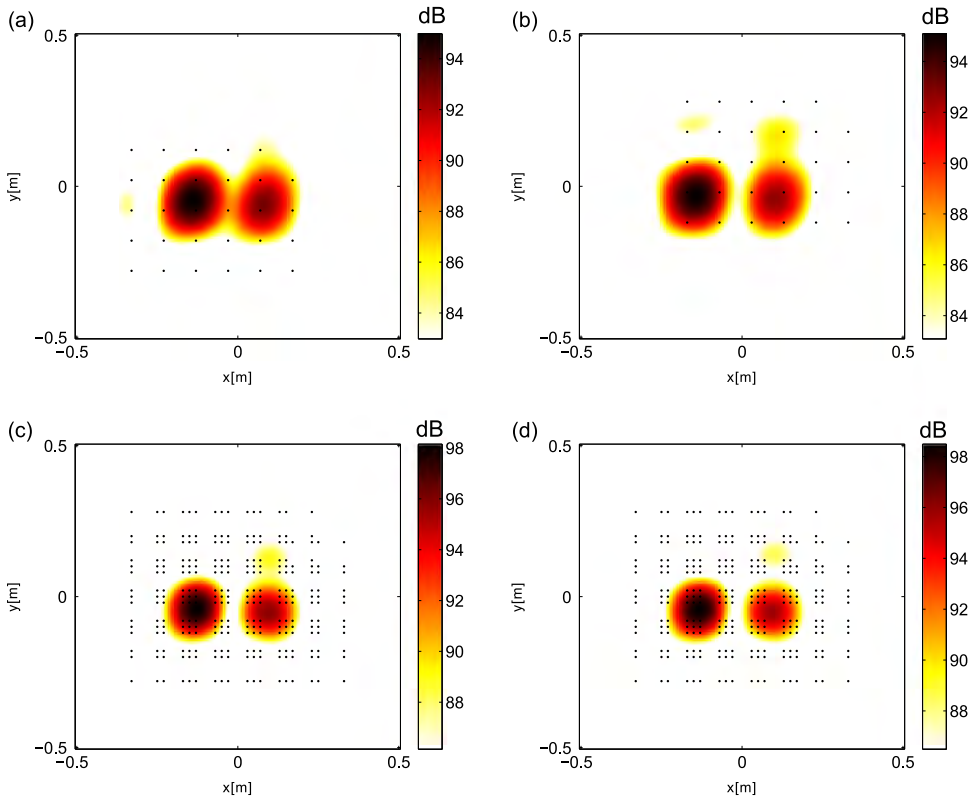

Fig. 14. (a, b) Acoustical source reconstruction at 3000 Hz for different fixed positions of the array (only two positions of sequential measurements are illustrated) compared with (c) and (d) (microphone positions are denoted by black bullets), (c) the MS method, and (d) the CP method.

are shown in Fig. 13(b). It is seen that MCE increases with frequency, while the relative error of source reconstruction is lower than 0.3151 in the whole frequency range. The results show that CP without reference can achieve comparable performance as the MS (with three references) for acoustical source reconstruction even though the matrix completion results may differ. Figs. 14 and 15 show the acoustical source reconstruction results at 3000 Hz and 6000 Hz respectively. It is seen that for a fixed position of the array, the reconstructed sources suffer from limited spatial resolution at low frequencies and their magnitudes are seriously underestimated at high frequencies. Incidentally, the allowable maximum frequency resolution provided by the prototype array is 1700 Hz. Fig. 14(d) and Fig. 15(d) show the source reconstruction result by CP, where at least two sources are well reconstructed even at a high frequencies about 6000 Hz which greatly extends the maximum working frequency for a fixed position of the array. Its results are comparable with the MS method. All these experimental results demonstrate that the CP method can be successfully applied to realize sequential measurements without references, and they can obtain very competitive results as compared with the MS method in the setup of with references.

7. Conclusion

The problem of sequential measurements without or with a limited number of references has been investigated. The main issue is that the phase relationships between consecutive snapshots are missing and results in missing entries in the spectral matrix. The approach proposed in this paper boils down to a spectral matrix completion problem subject to low rank constraint and is solved by proposed Cyclic Projection. This method clearly outperforms the referenced based method when the number of references is less than the number of uncorrelated sources and/or in the presence of noise on the references. CP has been proven to be quite robust in a variety of scenarios. One limitation of the CP method is the need for a priori selection of the rank of the spectral matrix, an issue which will be more deeply investigated in a future work.

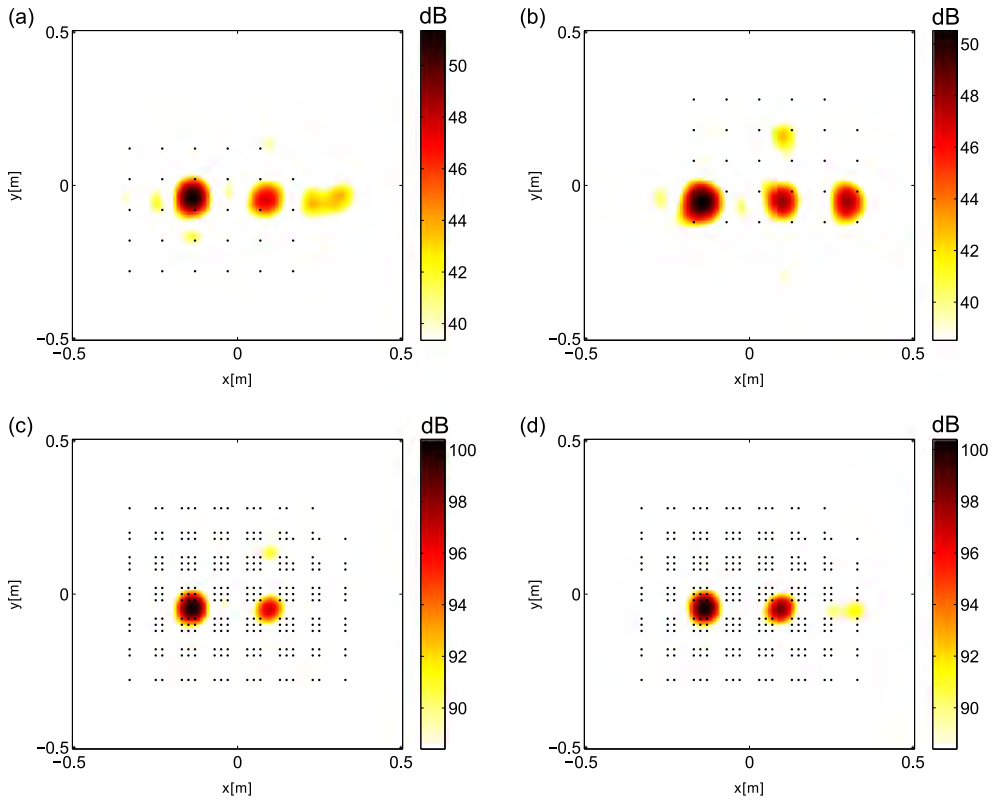

Fig. 15. (a, b) Acoustical source reconstruction at 6000 Hz for different fixed positions of the array (only two positions of sequential measurements are illustrated) compared with (c) and (d) (microphone positions are denoted by black bullets), (c) the MS method, and (d) the CP method.

Acknowledgments

This work was conducted in the framework of the LabEx CeLyA ("Centre Lyonnais d'Acoustique", ANR-10-LABX-60). The authors would like to thank the China Scholarship Council (CSC) for the financial support, and the continuous discussion with Dr. Antonio Pereira (Laboratoire Vibrations Acoustique, INSA de Lyon) and Professor Ivan Markovsky (Department ELEC Vrije Universiteit Brussel).

References

[1] E.G. Williams, *Fourier Acoustics: Sound Radiation and Nearfield Acoustical Holography*, Academic Press, New York, 1999.
[2] Y.-B. Zhang, F. Jacobsen, C.-X. Bi, X.-Z. Chen, Patch near field acoustic holography based on particle velocity measurements, *The Journal of the Acoustical Society of America* 126 (2) (2009) 721–727.
[3] R. Scholte, I. Lopez, N.B. Roozen, H. Nijmeijer, Truncated aperture extrapolation for fourier-based near-field acoustic holography by means of border-padding, *The Journal of the Acoustical Society of America* 125 (6) (2009) 3844–3854.
[4] E.G. Williams, Continuation of acoustic near-fields, *The Journal of the Acoustical Society of America* 113 (3) (2003) 1273–1281.
[5] K. Saijyou, S. Yoshikawa, Reduction methods of the reconstruction error for large-scale implementation of near-field acoustical holography, *The Journal of the Acoustical Society of America* 110 (4) (2001) 2007–2023.
[6] M. Lee, J.S. Bolton, Reconstruction of source distributions from sound pressures measured over discontinuous regions: *multipatch holography and interpolation*, *The Journal of the Acoustical Society of America* 121 (4) (2007) 2086–2096.
[7] J.-C. Pascal, S. Paillasseur, J.-H. Thomas, J.-F. Li, Patch near-field acoustic holography: *regularized extension and statistically optimized methods*, *The Journal of the Acoustical Society of America* 126 (3) (2009) 1264–1268.
[8] K. Saijyou, Regularization method for the application of k-space data extrapolation to near-field acoustical holography, *The Journal of the Acoustical Society of America* 116 (1) (2004) 396–404.
[9] M. Lee, J.S. Bolton, A one-step patch near-field acoustical holography procedure, *The Journal of the Acoustical Society of America* 122 (3) (2007) 1662–1670.
[10] M.R. Bai, C.-C. Chen, Application of convex optimization to acoustical array signal processing, *Journal of Sound and Vibration* 332 (25) (2013) 6596–6616.
[11] N. Chu, A. Mohammad-Djafari, J. Picheral, Robust Bayesian super-resolution approach via sparsity enforcing a priori for near-field aeroacoustic source imaging, *Journal of Sound and Vibration* 332 (18) (2013) 4369–4389.
[12] G. Chardon, L. Daudet, A. Peillot, F. Ollivier, N. Bertin, R. Gribonval, Near-field acoustic holography using sparse regularization and compressive sampling principles, *The Journal of the Acoustical Society of America* 132 (3) (2012) 1521–1534.
[13] A.V. Oppenheim, J.S. Lim, The importance of phase in signals, *Proceedings of the IEEE* 69 (5) (1981) 529–541.

[14] E.J. Candes, T. Strohmer, V. Voroninski, Phaselift: *exact and stable signal recovery from magnitude measurements via convex programming, Communications on Pure and Applied Mathematics* 66 (8) (2013) 1241–1274.
[15] Q. Leclere, Multi-channel spectral analysis of multi-pass acquisition measurements, *Mechanical Systems and Signal Processing* 23 (5) (2009) 1415–1422.
[16] J.S. Bendat, A.G. Piersol, *Engineering Applications of Correlation and Spectral Analysis*, Vol. 315, Wiley-Interscience, New York, 1980, p. 1.
[17] S. Yoon, P. Nelson, A method for the efficient construction of acoustic pressure cross-spectral matrices, *Journal of Sound and Vibration* 233 (5) (2000) 897–920.
[18] T. Loyau, J.-C. Pascal, P. Gaillard, Broadband acoustic holography reconstruction from acoustic intensity measurements. I: Principle of the method, *The Journal of the Acoustical Society of America* 84 (5) (1988) 1744–1750.
[19] C.-X. Bi, W.-Q. Jing, Y.-B. Zhang, Broadband acoustic holography from intensity measurements with a three-dimensional pressure-velocity probe, *The Journal of the Acoustical Society of America* 138 (5) (2015) 2929–2936.
[20] A. Nejade, Reference-less acoustic holography techniques based on sound intensity, *Journal of Sound and Vibration* 333 (16) (2014) 3598–3608.
[21] J. Antoni, Y. Liang, Q. Leclère, Reconstruction of sound quadratic properties from non-synchronous measurements with insufficient or without references: *proof of concept*, *Journal of Sound and Vibration* 349 (2015) 123–149.
[22] A. Tarantola, *Inverse Problem Theory and Methods for Model Parameter Estimation*, SIAM, Philadelphia, 2005.
[23] J. Antoni, A Bayesian approach to sound source reconstruction: *optimal basis, regularization, and focusing*, *The Journal of the Acoustical Society of America* 131 (4) (2012) 2873–2890.
[24] E. Candès, B. Recht, Exact matrix completion via convex optimization, *Foundations of Computational Mathematics* 9 (6) (2009) 717–772.
[25] S. Boyd, J. Dattorro, *Alternating Projections, Lecture Notes of EE 392 o*, Stanford University, Autumn Quarter 2004.
[26] I. Markovsky, *Low Rank Approximation: Algorithms, Implementation, Applications, Communications and Control Engineering*, Springer, London, 2012.
[27] E.J. Candès, X. Li, Y. Ma, J. Wright, Robust principal component analysis? *Journal of the ACM* 58 (3) (2011) 11.
[28] M. Elad, *Sparse and Redundant Representations: from Theory to Applications in Signal and Image Processing*, Springer, New York, 2010.
[29] G.N. Lilis, D. Angelosante, G.B. Giannakis, Sound field reproduction using the lasso, *IEEE Transactions on Audio, Speech, and Language Processing* 18 (8) (2010) 1902–1912.
[30] D. Malioutov, M. Çetin, A.S. Willsky, A sparse signal reconstruction perspective for source localization with sensor arrays, *IEEE Transactions on Signal Processing* 53 (8) (2005) 3010–3022.
[31] M. Fazel, Matrix Rank Minimization with Applications, PhD Thesis, Stanford University, 2002.
[32] B. Recht, M. Fazel, P.A. Parrilo, Guaranteed minimum-rank solutions of linear matrix equations via nuclear norm minimization, *SIAM Review* 52 (3) (2010) 471–501.
[33] X. Zhou, C. Yang, H. Zhao, W. Yu, Low-rank modeling and its applications in image analysis, arXiv preprint arXiv:1401.3409.
[34] M.S. Kompella, P. Davies, R.J. Bernhard, D.A. Ufford, A technique to determine the number of incoherent sources contributing to the response of a system, *Mechanical Systems and Signal Processing* 8 (4) (1994) 363–380.
[35] R. Salakhutdinov, A. Mnih, Bayesian probabilistic matrix factorization using Markov chain Monte Carlo, *Proceedings of the 25th International Conference on Machine Learning, ICML '08*, ACM, New York, NY, USA, 2008, pp. 880–887.
[36] C.M. Bishop, et al., *Pattern Recognition and Machine Learning*, Vol. 1, Springer, New York, 2006.
[37] E. Candes, Y. Plan, Matrix completion with noise, *Proceedings of the IEEE* 98 (6) (2010) 925–936.
[38] D.M. Photiadis, The relationship of singular value decomposition to wave-vector filtering in sound radiation problems, *The Journal of the Acoustical Society of America* 88 (2) (1990) 1152–1159.
[39] W. Cheney, A.A. Goldstein, Proximity maps for convex sets, *Proceedings of the American Mathematical Society* 10 (3) (1959) 448–450.
[40] P.L. Combettes, The foundations of set theoretic estimation, *Proceedings of the IEEE* 81 (2) (1993) 182–208.
[41] A.S. Lewis, D.R. Luke, J. Malick, Local linear convergence for alternating and averaged nonconvex projections, *Foundations of Computational Mathematics* 9 (4) (2009) 485–513.
[42] M. Fazel, H. Hindi, S. Boyd, Rank minimization and applications in system theory, *Proceedings of the 2004 American Control Conference*, Vol. 4, IEEE, Boston, 2004, pp. 3273–3278.
[43] A. Kyrillidis, V. Cevher, Matrix recipes for hard thresholding methods, *Journal of Mathematical Imaging and Vision* 48 (2) (2014) 235–265.
[44] P. Jain, R. Meka, I.S. Dhillon, Guaranteed rank minimization via singular value projection, in: *Advances in Neural Information Processing Systems*, 2010, pp. 937–945.
[45] M. Wax, T. Kailath, Detection of signals by information theoretic criteria, *IEEE Transactions on Acoustics, Speech and Signal Processing* 33 (2) (1985) 387–392.
[46] A. Pereira, J. Antoni, Q. Leclre, Empirical Bayesian regularization of the inverse acoustic problem, *Applied Acoustics* 97 (2015) 11–29.